Analytica Chimica Acta 1101 (2020) 157–168

Contents lists available at ScienceDirect

Analytica Chimica Acta

journal homepage: www.elsevier.com/locate/aca

Instantaneous trace detection of nitro-explosives and mixtures with nanotextured silicon decorated with Ag–Au alloy nanoparticles using the SERS technique

Sree Satya Bharati Moram [a], Abdul Kalam Shaik [a], Chandu Byram [a], Syed Hamad [b, *], Venugopal Rao Soma [a, *]

[a] Advanced Centre of Research in High Energy Materials (ACRHEM), University of Hyderabad, Hyderabad, 500046, Telangana, India
[b] The Guo China-US Photonics Laboratory, State Key Laboratory of Applied Optics, Changchun Institute of Optics, Fine Mechanics and Physics, Chinese Academy of Sciences, Changchun, 130033, China

HIGHLIGHTS

- SERS substrates developed by combining nanotextured Si and Ag–Au alloy NPs.
- Trace level detection of explosives achieved using portable Raman spectrometer.
- LOD of ~5 pM, ~36 nM, and ~400 nM achieved for MB, PA, and RDX, respectively.
- Reproducible SERS measurements of binary, tertiary explosive mixtures.

GRAPHICAL ABSTRACT

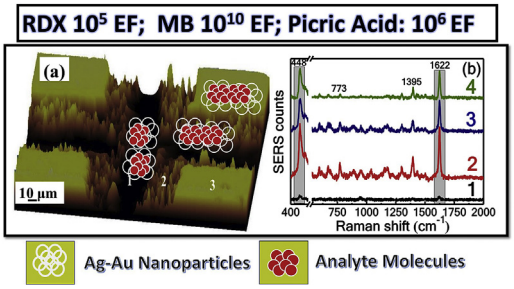

ARTICLE INFO

Article history:
Received 4 October 2019
Received in revised form
12 November 2019
Accepted 10 December 2019
Available online 16 December 2019

Keywords:
Surface-enhanced Raman scattering
Femtosecond laser ablation
Ag–Au alloy NPs
Methylene blue
Explosives detection

ABSTRACT

The development of recyclable surface enhanced Raman scattering (SERS) based sensors has been in huge demand for trace level explosives detection. A simple, hybrid Silicon (Si) nanotextured target-based SERS platform is fabricated through patterning micro square arrays (MSA) on Si using femtosecond (fs) laser ablation technique at different fluences. Using the hybrid target Si MSA substrate loaded/decorated with Ag–Au alloy NPs (obtained using femtosecond ablation in liquids) we demonstrate the trace level detection of organic nitro-explosives [picric acid (PA), 2,4-dinitrotoluene (DNT), and 1, 3, 5-trinitroperhydro-1, 3, 5-triazine (RDX)] and their mixtures. The microstructures/nanostructures of MSA fabricated at an input fluence of 9.55 J/cm^2, and decorated with Ag–Au alloy NPs, exhibited exceptional SERS enhancement factors (EFs) up to ~10^{10} for MB, ~10^6 for PA, and ~10^4 for RDX with the detection limits obtained being ~5 pM, ~36 nM, and ~400 nM for MB, PA and RDX respectively. Furthermore, we demonstrate these SERS substrates possess good reproducibility (RSD values < 15%) and a superior performance compared to a commercial Ag substrate (SERSitive, Poland). Three binary mixtures, i.e. MB-PA, MB-DNT, PA-DNT at different concentrations, were also investigated using the same SERS substrate to test the efficacy. Further, the SERS spectra of dyes, explosives, and complex mixtures were utilized for discrimination/classification using principal component analysis.

* Corresponding authors.
E-mail addresses: siddu.hamad@gmail.com (S. Hamad), soma_venu@uohyd.ac.in, soma_venu@yahoo.com (V.R. Soma).

https://doi.org/10.1016/j.aca.2019.12.026
0003-2670/

1. Introduction

Raman spectroscopy is a widely used analytical technique in various fields for material analysis such as food processing, modern biology, medicine, and detection of explosives due to its capability to provide fingerprint response [1–5]. Because of its weak intrinsic Raman scattering, a derived technique of Raman spectroscopy called surface-enhanced Raman scattering (SERS) has been pursued over the past two decades in which the scattered Raman intensity is enhanced using surface metal nanostructures [6,7]. SERS technique has been demonstrated to be an efficient and practical way of detecting explosive molecules. In SERS technique, the Raman signal of an analyte is manifested due to the (i) strong electromagnetic (EM) enhancement in the vicinity of plasmonic nanostructures (NSs)/nanoparticles (NPs) and (ii) a weak chemical enhancement (CM) as a consequence of charge transfer between the substrate and the analyte molecules. Many SERS studies were performed using noble metal nanomaterials (NSs/NPs) deposited on plain Silicon (Si) or glass substrates as a base/support through exploitation of the induced localized surface plasmon resonance (LSPR) [8–13]. However, few metal-less 2D-materials such as graphene, MoS_2, WSe_2, Si/SiO_x, etc. have been shown to contribute to SERS signal through chemical enhancement [14–16]. Consequently, integrating semiconductor (Si/SiO_x), an excellent low-cost material, with the plasmonic NPs could possibly exploit both the EM and CM enhancements and such studies are of huge interest towards development or practical SERS substrates. In line with this, substantial efforts are being directed towards modifying the base/support itself through fabricating Si nano/micropillars/pyramids using various methods including e-beam lithography, etching, vapor deposition to improve Raman response [17–26]. However, most of these fabrication techniques include extended preparation time, considerable cost, and several processing steps. Femtosecond (fs) laser ablation is a powerful yet unpretentious technique to fabricate rapid and robust microstructure/nanostructures on various targets. Nevertheless, the surface morphology of the resulting NSs is influenced by laser parameters such as pulse duration, wavelength, and fluency and also on the properties of surrounding medium (air/liquid/buffer gas). Only a few works have discussed the process of manufacturing Si SERS substrates in a single and two-step process using fs ablation. Lin et al. [27] followed a one-step process: fs laser ablation of Si in $AgNO_3$ solution to fabricate Ag adsorbed Si substrates whereas Yang et al. [28] demonstrated a two-step approach: laser scanning microstructures/nanostructured Si followed by deposition of a silver thin film on the fabricated structures. Apart from surface texturing of base, various compositions of NPs made up of two or more compositions of plasmonic materials were synthesized to investigate the Raman response of analyte molecules [29–34]. Bi et al. observed ~20 times enhancement in the SERS signal using bimetallic gold-silver nanoplate arrays than that of the gold nanoplate arrays [35]. In particular, the fabrication of Ag–Au alloy NPs has received lot of attention due to their tunable LSPR characteristics through combining the individual properties associated with Ag (superior plasmonic nature comapred to Au) and Au (higher stability comapred to Ag) for obtaining superior SERS response. Recently, we fabricated different alloy NPs (Ag–Au, Ag–Cu, and Cu–Au) followed by detailed SERS studies found that Ag–Au NPs coated plain Si substrate have indeed exhibited superior SERS performance for detecting MB (5 nM), PA (5 μM) and DNT (5 μM) with the EFs of ~10^7, ~10^4, and ~10^4, respectively [29,36].

Herein, we utilized the effect of micro square arrays (MSA) fabricated on Si in the air at different fluences (3.18–31.84 J/cm^2) and Ag–Au alloy NPs to enhance the SERS performance. The fabricated SERS substrates were characterized by field emission scanning electronic microscopy (FESEM) and energy dispersive spectroscopy (EDX) mapping techniques. Significantly, the Si MSA substrate fabricated at 9.55 J/cm^2, coated with Ag–Au alloy NPs has shown the best SERS enhancement for MB molecule (10^{-11} M) compared with other MSA substrates due to the generation of a large number of hotspots, resulting in the strongly localized surface plasmons. The above-mentioned substrate was then used to probe the explosive molecules (PA, RDX) in pure form. Majority of the earlier SERS studies were using (a) non-explosive molecules (b) confined to the detection of either one or two analyte molecules. Further, very few studies focused on detection of analytes in mixtures (binary or ternary). A few SERS studies though have focused on the detection of individual explosive molecules, but in real-time, the samples will, generally, be present in a complex mixture form. Therefore, we extended our work to detect explosive mixture with various concentrations (PA-MB, DNT-MB, PA-DNT, and MB-PA-DNT) through observing fingerprint response offered in SERS technique. Furthermore, the principal component analysis (PCA) technique was utilized to group/classify the explosives, explosive-dye mixture and explosive-explosive mixture by analyzing the SERS spectra. Our experimental results showed that these Si NSs loaded with Ag–Au alloy NPs provided good sensitivity and reproducibility for all the molecules, even in the form of mixtures.

2. Materials and methods

2.1. Chemicals and reagents

A Si wafer [p-type crystalline Si (100)], silver target of 1 mm thickness (>99% pure, Sigma Aldrich), tetrachloroauric (III) acid ($HAuCl_4$ $4H_2O$) ≥99.9% trace metals basis, methanol (reagent grade), acetonitrile (reagent grade), acetone (reagent grade), and the methylene blue dye molecule [MB; $C_{16}H_{18}ClN_3S$], Malachite green [MG: $C_{23}H_{25}N_2$] were purchased from Sigma Aldrich. The explosive molecules of 2,4,6-trinitrophenol (Picric Acid; PA; $C_6H_3N_3O_7$), 2,4-dinitrotoluene (DNT; $C_7H_6N_2O_4$) and 1, 3, 5-trinitroperhydro-1, 3, 5-triazine (RDX; $C_3H_6N_6O_6$) were provided by HEMRL (Pune, India) for detection.

2.2. Fabrication of silicon microstructures/nanostructures

Fig. 1(a) depicts the schematic of MSA fabrication on Si by fs laser ablation in air. The ablation experiments were performed using Ti: sapphire laser system (LIBRA, 4W, M/s Coherent, USA) delivering pulses of ~50 fs duration, at a central wavelength of 800 nm and 1 kHz repetition rate. Before ablation, the Si targets were cleaned in an ultrasonic bath with acetone and ethanol to remove any surface impurities. A combination of half-wave plate and Brewster polarizer was used to control the incident pulse energy. Five different pulse energies, i.e., 10 μJ, 20 μJ, 30 μJ, 50 μJ, and 100 μJ (higher than the ablation threshold of Si ~1.5 J/cm^2 [37]), were utilized to fabricate the Si microstructure/nanostructures. The laser beam (with an input diameter of ~10 mm) was focused onto the sample using a convex lens of 10 cm focal length. The estimated fluences were 3.18 J/cm^2, 6.36 J/cm^2, 9.55 J/cm^2, 15.92 J/cm^2 and 31.84 J/cm^2 for five different energies of 10 μJ, 20 μJ, 30 μJ, 50 μJ and 100 μJ, respectively. The Si samples were mounted on a high

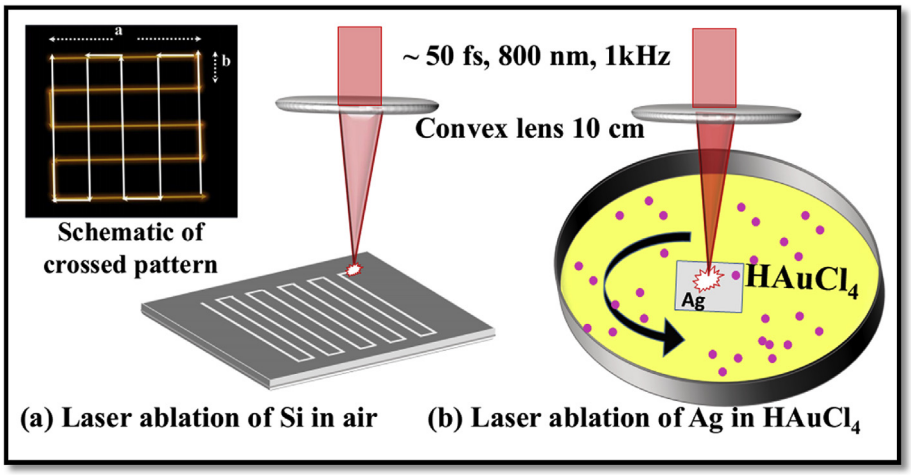

Fig. 1. Schematic of experiment details (a) fs laser ablation of Si in air (b) synthesis of Ag–Au alloy NPs. [Inset shows the micro square array (MSA) fabricated on Si].

precision computer-controlled two-axis translation stage. It was utilized to draw lines with scanning speeds of 0.1 and 0.1 mm/s in both X- and Y-directions through a raster scanning procedure starting at two different positions resulting in MSA over 5 × 5 mm^2 area. The inset in Fig. 1 illustrates the scanning path/interaction of the laser beam on the Si substrate; in this image 'a' is the length of the scanning lines (5 mm), and 'b' is the spacing between two adjacent scanning lines (50 μm). Every laser scanning line turns into a single groove. Hence, line-by-line scanning procedure provides an array of grooves. Following the laser interaction, all the patterned surfaces or MSA were rinsed in deionized water and acetone to remove the dust particles and organic contaminants and were preserved at room temperature.

2.3. Fabrication of Ag–Au alloy NPs

Fig. 1(b) [right] depicts the schematic of Ag–Au alloy NPs fabrication by fs laser ablation of Ag target in $HAuCl_4$ solution at 300 μJ pulse energy. The detailed fabrication procedure of Ag–Au NPs was reported in our earlier study [36], and the formation mechanism is briefly discussed as follows: The interaction of intense fs laser pulses with the precursor ($HAuCl_4$) results in the formation of $AuCl_4^-$ ions owing to their higher reduction potentials [$HAuCl_4 + H_2O + n\ h\nu \rightarrow AuCl_4^- + H^+ + OH^-$, $AuCl_4^- + 3e^- \rightarrow Au^0 + 4Cl^-$]. The ablation of Ag target results in the formation of plasma owing to the instantaneous heating and vaporization of Ag target in the focal region. As the time progresses, plasma plume cools down, and transmission of energy to the surrounding medium triggers the formation of the cavitation bubble [containing both the ablated matter (Ag) and the liquid-vapor (Au)], which expands and finally collapses due to the extreme conditions of high pressure and high temperature gradient. This condition leads to a replacement reaction between ablated Ag and Au ions [$Ag^* + Au^* \rightarrow AgAu^*$], resulting in the formation of Ag–Au alloy NPs [36,38].

2.4. Instrumentation and characterization

The Si MSA fabricated through laser ablation in the air was characterized using FESEM [Carl ZEISS instrument] technique. The energy-dispersive X-ray analysis (EDAX) was utilized to check the constituent elements on Si MSA. Furthermore, the Si MSA was again characterized by FESEM for the mapping of Si, Ag, and Au after drop-casting the Ag–Au alloy NPs (~20 μL). The effect of surface morphology on Si MSA in the presence of Ag–Au NPs was examined by model LabRAM (Horiba Jobin Yvon-632 nm) spectrometer by probing MB. Except for this, all other Raman measurements were performed using a portable Raman spectrometer ($\lambda_{excitation}$ = 785 nm, M/s B&W Tek, I-Raman plus, USA). A laser power of 30 mW was used to record SERS spectra of various analyte molecules, and each SERS spectrum is a result of 3 accumulations with an acquisition time of 5 s.

2.5. SERS substrates preparation

The stock solution of MB (0.1 M), PA (0.1 M), and RDX (0.1 M) were prepared in ethanol, methanol, and acetonitrile. Subsequently, these solutions were diluted to achieve various concentrations (ranging from 1 mM to 10 pM). While making the complex mixture solutions, samples with equal volumes but same/different concentrations were mixed in an ultrasonic bath for 10 min. The SERS substrates were prepared by drop-casting 20 μL of Ag–Au alloy NPs solution on cleaned Si MSA substrates. Later 20 μL of the analyte molecule of interest was dropped on these SERS substrates for performing SERS measurements.

3. Results and DISCUSSIONS

3.1. Characterization of the Si MSA (FESEM and EDX)

Fig. 2(a)-(e) and 2(f)-2(j) illustrate the lower and higher magnification FESEM micrographs of Si MSA fabricated at 3.18, 6.36, 9.55, 15.92 and 31.84 J/cm^2. A typical sequence of magnified images depicting the edge morphology of Si MSA obtained at a fluence of 3.18 J/cm^2 is shown in Fig. S1 of the supporting information (SI). From Figs. 2(f)-2(j) it is evident that semi-spherical shaped Si/SiO_X NPs with fewer voids were obtained at the first two fluences 3.18 and 6.36 J/cm^2 while semi-spherical and rod-shaped Si/SiO_X NPs with more nanocavities, gaps, etc. were observed at 9.55 J/cm^2 [Fig. 2(h)]. At higher fluences, large-sized spherical shaped Si/SiO_X NPs with distracted microstructures on Si MSA were observed. The sizes and shapes of the NPs produced in laser ablation with fs pulses depend on the origination of thermo-elastic waves below the surface layer, where the phase explosion (or) coulomb explosion [39] occurs depending on the metallic or dielectric nature of the substance. However, the complete mechanism of phase explosion (or) coulomb explosion associated with thermo-elastic wave succeeded by NPs generation is not entirely understood [40,41]. We believe and understand from the existing literature that low laser fluences

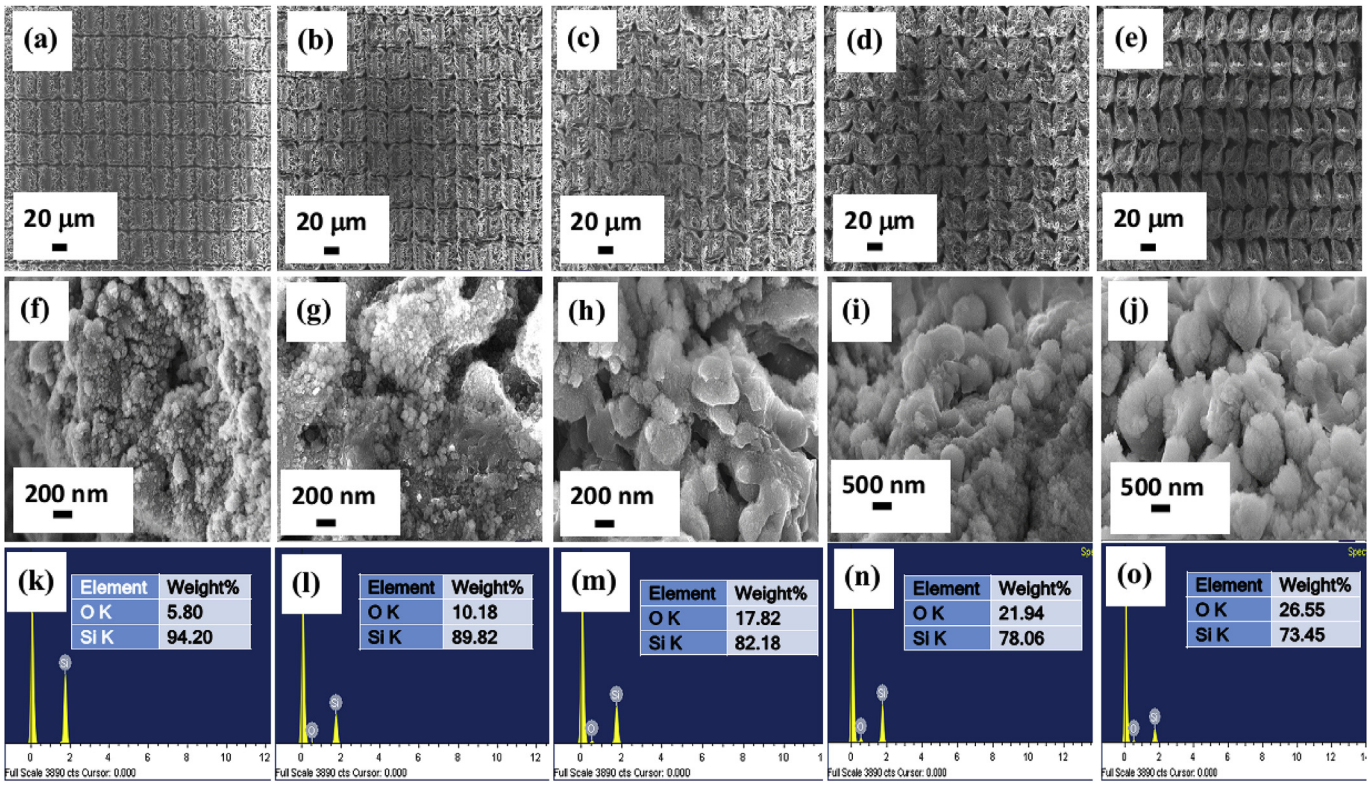

Fig. 2. FESEM images of fs laser fabricated MSA on Si substrates at different fluences (a) 3.18 (b) 6.36 (c) 9.55 (d) 15.92 and (e) 31.84 J/cm^2 with the scale bar of 20 µm and (f, g, h, i and j) present their corresponding high resolution images; (k, l, m, n and o) present the corresponding EDX images and insets show atomic weight% of the elements.

cause negative stress, which ultimately supports and strengthens the repelling force between the atoms, leading to the formation of small-sized Si/SiO_X NPs. However, in the case of higher laser fluences the repelling force will be stronger than the negative stress and bonds will be broken instantaneously, which may perhaps generate bigger sized Si/SiO_X NPs as well as increased nanostructure deformation/destruction due to the Coulomb explosion [40,41]. The laser ablation of Si in the ambient air leads to change in the chemical properties of its surface along with its physical properties due to the oxidation effect. During the laser ablation of Si target in air, the Si particles in plasma interact with the oxygen from the surrounding air and form SiO/SiO_X on the Si MSA. The Si substrates fabricated at different fluences were studied using EDX spectroscopy to measure the extent of oxidation on Si MSA. Fig. 2 (k)-2(o) depict the EDX spectra, and the inset of each depicts the Si and O weight percentages. The degree of oxidation on Si MSA was observed to increase as the fluence increased from 3.18 to 31.84 J/cm^2, which could probably be attributed to the increased atomization of oxygen from the surrounding air.

Further, the Si MSA (9.55 J/cm^2) was coated with Ag–Au alloy NPs and the distribution of these alloy NPs were inspected using FESEM- EDX mapping. Fig. 3 shows the EDX map of Si MSA decorated by Ag–Au alloy NPs and the elemental distribution of each constituent. Fig. 3(b) illustrates the overall mapping in a selected portion of the target. Fig. 3(c)–(e) represent the corresponding elemental mapping images of elemental Si (red colour), Ag (yellow colour), and Au (green colour) on the Si MSA. Fig. 3(f) depicts the EDX spectra while the inset shows the table representing the weight percentage of each individual element. The deposited Ag–Au NPs on Si NSs will be able to create multiple hot spots, leading to the excitation of strongly localized surface plasmons resulting in huge enhancements of the SERS signal.

4. SERS studies

4.1. Detection of a dye molecule

To establish the combined effect of Si MSA as well as Ag–Au alloy NPs towards SERS enhancement, the target was studied region-wise using a micro-Raman spectrometer (LabRAM, Horiba Jobin Yvon) at 632 nm excitation wavelength. Later SERS studies (on explosive molecules) presented in this work have been performed using a portable Raman spectrometer, which is easier and practical to transport to the point of interest (field). The micro-Raman spectrometer, however, helped us in understanding the surface morphology and identifying the interesting portions of substrates where the enhancement is higher. MB was chosen as a probe molecule to study the effect of microstructure/nanostructure in the SERS signal. The maximum SERS signal was observed from the edges of MSA because of the micro-protrusions and/or nanocavities originating from the redistribution of ablated mass in comparison to the regions inside the groove and non-irradiated portions of Si. The detailed SERS measurements performed in the various areas are illustrated in Fig. S2 of the SI.

4.2. Detection of MB from different Si MSA substrates

We have also recorded the SERS spectra of MB (5 nM) using a portable Raman spectrometer with an excitation source at 785 nm from the Ag–Au alloy NPs deposited on plain Si [Fig. 4(a)(i)] and Si MSA. The normal Raman spectra of MB (0.1 M) on the plain Si (without NPs) was shown in Fig. 4(a) [pink colour]. The SERS optimization measurements were performed on Si MSA fabricated at five different laser fluences to investigate and understand the effect of their morphology/roughness in SERS

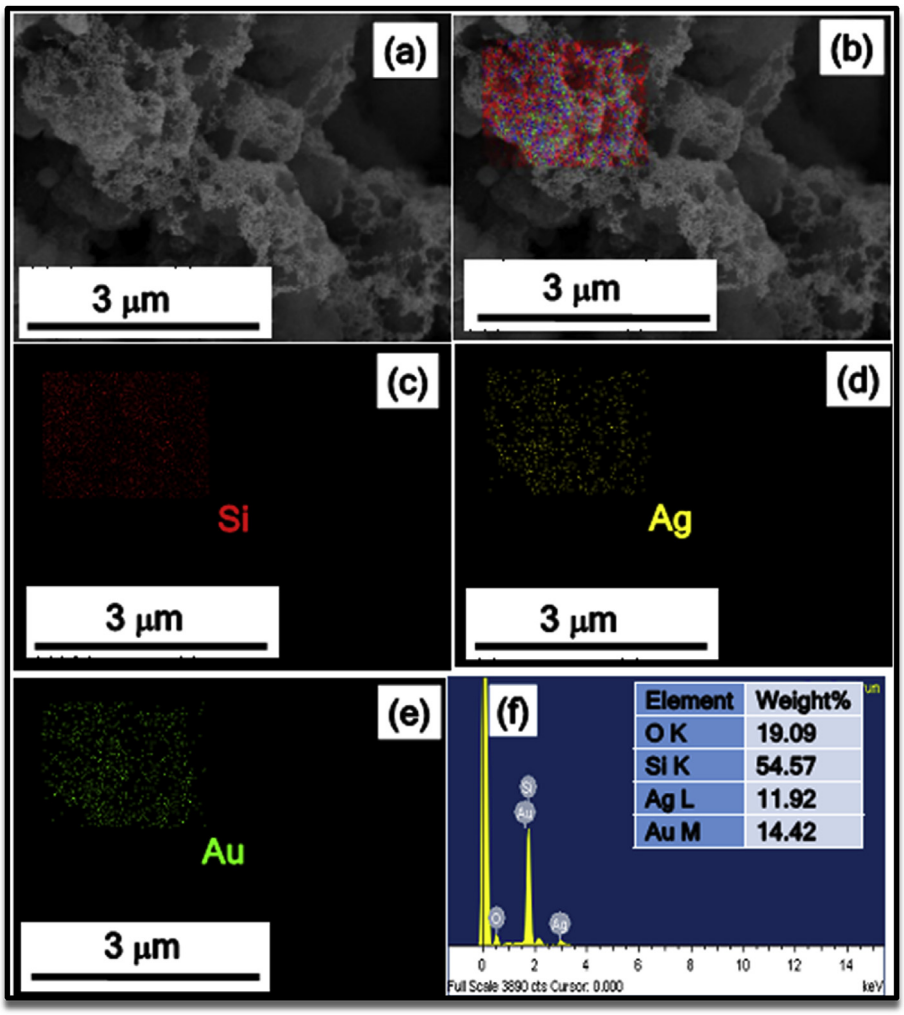

Fig. 3. (a) FESEM image of edges of Si MSA fabricated at 9.55 J/cm^2 and (b-e) EDX elemental mapping of Ag–Au alloy NPs deposited on Si MSA fabricated at 9.55 J/cm^2 (c) Si (d) Ag (e) Au (f) EDX spectra inset shown the atomic weight % of elements.

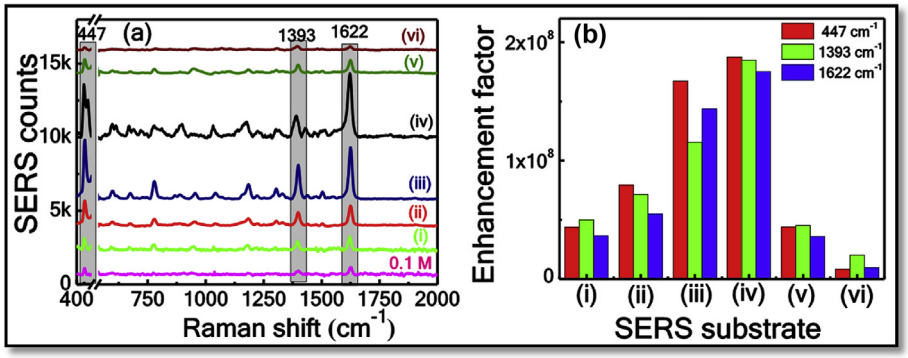

Fig. 4. (a) SERS spectra of MB (5 nM) adsorbed on Ag–Au alloy NPs decorated on (i) bare Si and Si MSA fabricated at different fluences (ii) 3.18, (iii) 6.36, (iv) 9.55, (v) 15.92 and (vi) 31.84 J/cm^2 and, (b) The histogram of EF from all the substrates. The Raman spectra MB (0.1 M) is shown in pink colour (bottom spectra). (For interpretation of the references to colour in this figure legend, the reader is referred to the Web version of this article.)

activity. The obtained SERS spectra from all the substrates with Ag–Au alloy NPs and are shown in Fig. 4(a) (ii) - (vi). From the figure, it is evident that the Raman intensity increased as the fluence increased from 3.18 to 9.55 J/cm^2, and then it decreased for a further increase in the fluence from 15.92 to 31.84 J/cm^2. The enhancement factor (EF) using the following relation EF = $(I_{SERS} \times C_R)/(I_R \times C_{SERS})$, where I_{SERS} and I_R are the Raman signal intensity of the SERS substrate and bare silicon and, C_{SERS} and C_R are the concentration of the analyte molecule on the SERS substrate and bare silicon. The EF calculation process can be found in

the previous reports [42,43]. The EFs of three modes of MB i.e., 447, 1393 and 1622 cm^{-1} from all the substrates were calculated and are illustrated in Fig. 4(b). The EFs obtained for 1622 cm^{-1} peak were 3.64 × 10^7, 5.46 × 10^7, 1.43 × 10^8, 1.75 × 10^8, 3.58 × 10^7 and 9.53 × 10^6 for plain Si with NPs and Si MSA at fluence 3.18, 6.36, 9.55, 15.92 and 31.84 J/cm^2 with NPs respectively. With the increased fluence from 3.18 to 6.36 J/cm^2, EF increased by 2.7 times and 3.2 times for 9.55 J/cm^2. Later it was observed that the EF decreased to 0.65 and 0.18 times for fluences of 15.92 and 31.84 J/cm^2 when compared to that of the EF obtained at a fluence of 3.18 J/cm^2. A similar trend was also observed in the EFs of two other modes. Si MSA obtained at 9.55 J/cm^2 exhibited the optimum SERS signals in comparison to the other Si MSA substrates. This could be ascribed to (i) the presence of semi-spherical and rod-shaped Si/SiO_X NPs with larger quantity of nano-voids/gaps etc., which could possibly have accommodated a higher number of Ag–Au alloy/bimetallic NPs (ii) aggregation of NPs over the edge of MSA leading to the formation of again a higher number of hot spots and (iii) modifications of local fields under the influence of shape and size of the nanostructure which enhance the scattering efficiency. Subsequently, the Si MSA fabricated at 9.55 J/cm^2 was utilized to perform SERS studies because of its superior SERS activity.

4.3. Sensitivity and reproducibility studies of the optimized substrate

For the real-time/practical applications, a stable and reproducible response is mandated from the SERS active substrates. It is expected that Ag–Au alloy NPs coated on a plain surface might be one of the conceivable substrates for SERS reproducibility studies. Here, SERS sensitivity and reproducibility have been investigated for the Au–Ag NPs dispersed on the Si MSA over a large area, fabricated at a fluence of 9.55 J/cm^2, as it exhibited the highest EFs in the present study. Fig. 5(a) shows the SERS spectra of MB at various concentrations (from 10^{-11} M to 10^{-6} M). It is evident from the data that 1622 cm^{-1} mode was decreased with decrease in concentration and is feebly observed at 10^{-11} M concentration. Thus, a sensitivity of picomolar (pM) concentration was achieved for MB dye molecule, corroborating the great sensitivity of the SERS active substrate. A linear dependence of SERS intensity with analyte concentration was verified by fitting log I versus log C plot by considering three major peaks of MB. Fig. 5(b) shows the linear plots of 447, 1393, and 1622 cm^{-1} modes with considerable R^2 values of ~0.99, ~0.98, and ~0.96, respectively, demonstrating a good linear variation of intensity versus concentration. To quantitatively characterize the SERS ability, we estimated the EFs of three

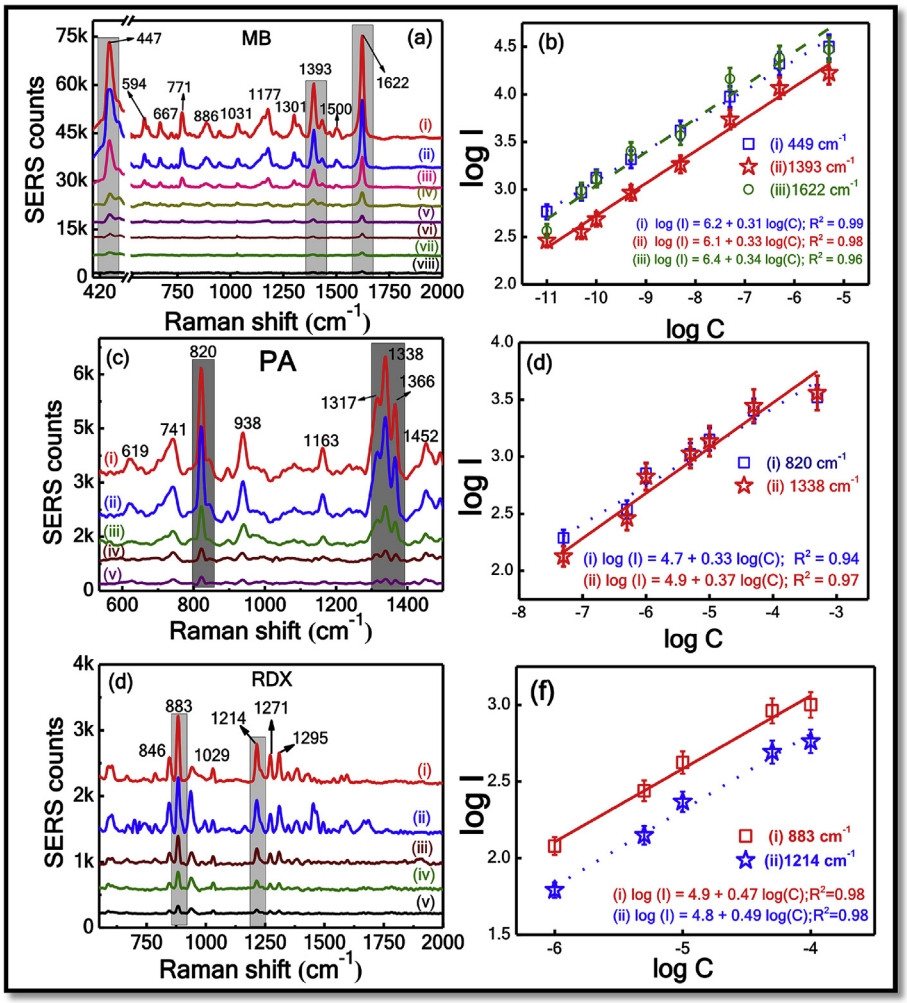

Fig. 5. SERS spectra of (a) MB [(i) 5 μM (ii) 500 nM (iii) 50 nM (iv) 5 nM (v) 500 pM (vi) 100 pM (vii) 50 pM and (viii) 10 pM] (c) PA [(i) 500 μM (ii) 50 μ M (iii) 5 μM (iv) 500 nM (v) 50 nM] (e) RDX [(i) 100 μM (ii) 50 μ M (iii) 10 μM (iv) 5 μM (v) 1 μM]. (b, d, and f) linear dependence log plots of Raman mode intensity vs. concentration for the major modes of MB, PA, and RDX, respectively.

major peaks of MB for 10^{-11}M, and the estimated EFs were 0.85×10^{10}, 1.2×10^{10}, and 1.2×10^{10} for 447, 1393 and 1622 cm^{-1} modes, respectively. The EFs reported in previous studies for the rigid SERS substrates and the EFs achieved in the present work are summarized in Table S1. The EFs accomplished in our case with Ag–Au alloy NPs decorated on Si MSA substrate indicates that this substrate could be used as an effective sensor for molecular detection at trace level. Apart from the sensitivity, reproducibility of the SERS targets is a significant concern owing to their robust usage. The reproducibility of the SERS substrate was demonstrated by recording the SERS signals of MB at 10 pM concentration. Fig. S3(a) of SI shows the SERS spectra of MB (10^{-11}M) recorded at 13 randomly selected places on the Ag–Au alloy NPs coated Si MSA. The intensity histograms for the three significant peaks observed at 447, 1393, and 1622 cm^{-1} with their respective RSD values of 6.52%, 13.1%, and 6.5%, shown in Fig. S3(b). The obtained results demonstrating high sensitivity as well as good reproducibility (RSD <15%) of Si MSA. This data suggests that the Au–Ag Alloy NPs coated Si MSA substrate can be considered as a potential SERS substrate for practical applications. Therefore, we have utilized the same substrate to detect the explosives and complex mixtures by following the simple cleaning procedure as given in SI [44].

4.4. Detection of explosive molecules

The versatility of the investigated SERS substrate was demonstrated by detecting and analysing explosive molecules in their pure form and in complex mixtures. Si MSA substrate fabricated at 9.55 J/cm^2 with Ag–Au alloy NPs was used to detect two different explosive molecules, i.e., PA and RDX, in their pure form at minimum concentrations. Fig. 5(c) shows the SERS spectra of PA with different concentration ranging from 500 μM to 50 nM i.e. (i) 500 μM (ii) 50 μ M (iii) 5 μM (iv) 500 nM (v) 50 nM. At lower concentration of PA (50 nM), only two major peaks, positioned at 820 $cm^{-1}$and 1338 cm^{-1}, were identified, as depicted in Fig. 5(c). Fig. 5(d) illustrates the linear variation in the SERS signal intensity of the 820 cm^{-1}, 1338 cm^{-1} modes versus analyte concentration (log plot) with correlation coefficients of 0.94 and 0.97, respectively. PA was detected even at 50 nM concentration with two major peaks at 820 cm^{-1} and 1338 cm^{-1} with their respective EFs being 2.2×10^6 and 0.8×10^6. A significant improvement (2-fold) was achieved in the sensitivity of explosive molecules and is apparent from comparison of the results obtained from this study (EF ~10^6) with the previous studies using Ag–Au alloy NPs on the plain Si as SERS active substrate (EFs of ~10^4) [36]. The reproducibility test was carried out at 14 random sites for PA, and the estimated RSD for the characteristic peak of PA at 820 cm^{-1} and 1338 cm^{-1} is 8.7% and 13.5%, shown in Fig. S4(a) of the SI. Besides high sensitivity, the SERS substrate also demonstrated good reproducibility.

Further, the SERS performance of the substrate (Ag–Au NPs coated Si MSA substrate at 9.55 J/cm^2) was verified by choosing RDX as the target analyte molecule [45]. There were no Raman spectra observed for 1 μM RDX molecule, which was adsorbed on Ag–Au alloy NPs with plain Si substrate (data not presented here). However, the Ag–Au alloy NPs coated Si MSA substrate has helped us to detect Raman signals even from 1 μM RDX analyte. The concentration-dependent SERS spectra of RDX from 100 to 1 μM [(i) 100 (ii) 50 (iii) 10 (iv) 5 (v) 1 μM] are shown in Fig. 5(e). The observed Raman modes of RDX are in good agreement with those reported previously [46]. The modes observed at 883 cm^{-1} and 1214 cm^{-1} in the SERS spectra of RDX were ascribed to C–N stretching and N–C stretching, respectively. It can be observed that the SERS signal intensity (883 and 1214 cm^{-1}) increased with the increase of the concentration of RDX. Fig. 5(f) illustrates the linear dependence of log plot intensity versus analyte concentration with a R^2 value of 0.98. The reproducibility of SERS spectra of RDX (50 μM) is depicted in Fig. S4(b) and corresponding histogram plots of 883 cm^{-1} and 1214 cm^{-1} peaks from 14 different spots with reasonable RSD values of 7.7% and 14.7%, respectively. Furthermore, the SERS spectra of malachite green (MG, a common dye molecule) were recorded on two optimized Si MSA substrates fabricated at 9.55 J/cm^2 to inspect the batch-to-batch reproducibility. The RSD in the SERS intensity of the 1614 cm^{-1} peak was utilized to investigate the batch-to-batch reproducibility and it was found to be <10% [data is presented in Figs. S5 (a-d) of the SI] [47].

Table 1
Summary of the EF's for different analyte molecules obtained in the present study.

S. No.	Analyte (Concentration)	Peak (cm^{-1})	EF
1	MB (1×10^{-11} M)	447	0.85×10^{10}
		1393	1.2×10^{10}
		1620	1.2×10^{10}
2	PA (5×10^{-8} M)	820	2.2×10^{6}
		1338	0.8×10^{6}
3	RDX (1×10^{-6} M)	883	9.3×10^{4}
		1214	7.5×10^{4}

SERS based Detection of Complex mixtures [PA-MB, PA-DNT].

The EFs estimated for the lowest detected concentrations of MB, PA, and RDX are listed in Table 1. These EFS are on-par/superior to the results obtained by our group [29,36,44,48–51]. To estimate the limit of detection (LOD) for all the three molecules investigated, the most prominent peaks of MB at 1622 cm^{-1}, PA at 822 cm^{-1} and RDX at 883 cm^{-1} were opted for analysis. Here, the LOD value was calculated using the formula LOD = 3σ/b, where 'σ' is the standard deviation of the blank and 'b' is the gradient of the linear equation. The slope "b" is obtained from the intensity versus concentration plots (illustrated in Fig. S6 of the SI). The estimated LOD values for the MB, PA, and RDX were ~5 pM, ~36 nM, and ~400 nM, respectively. The variations in EFs and LOD from sample to sample on the same substrate could possibly be attributed to the strong affinity and orientation of these molecules on the SERS substrate.

Apart from the sensitivity, selectivity (i.e., the ability of the technique to provide individual/specific response to various materials of interest) is also an important aspect in the explosive analysis. However, in real-time scenarios, the explosive samples inevitably coexist in mixed form with the multiple interferants. Thus, rendering the quantitative and qualitative detection of each molecule from the mixed form has been one of the most important and challenging applications of SERS. Here, we have utilized the same substrate, i.e. Ag–Ag NPs dispersed on Si MSA fabricated at 9.55 J/cm^2 to detect the explosive mixtures. Three binary mixtures/solutions were prepared with MB, PA, and DNT, i.e. PA-MB, DNT-MB, and PA-DNT at different concentrations by mixing the analyte solutions in equal volumes. Fig. 6(a) illustrates the SERS spectrum of PA (5 μM) + MB (5 nM) binary mixture in comparison with pure SERS spectra of PA (5 μM) and MB (5 nM). The SERS spectrum of PA + MB mixture consisted of vibrational modes of PA and MB. Similarly, the SERS spectra of second binary mixture comprising of a dye and an explosive molecule, i.e. MB-DNT (0.5 nM + 0.5 μM) were also recorded and as shown in Fig. 6(b). In the SERS spectra of mixture, the peaks were observed with small shift and with the decreased intensity. Further, the SERS spectra of PA-MB mixture were recorded by varying the MB concentration from 5 nM to 50 pM [(i) 5 nM (ii) 500 pM and (iii) 50 pM] at a fixed concentration of PA molecule (5 μM), as shown in Fig. 6(c). With the decreasing in the concentration of MB the intensity of characteristic peaks of MB (447, 1620 cm^{-1}) decreased as well, but the PA peak intensity (820 cm^{-1}) remains unchanged. Similarly, the concentration of PA was changed from 50 μM to 50 nM at a fixed concentration of MB

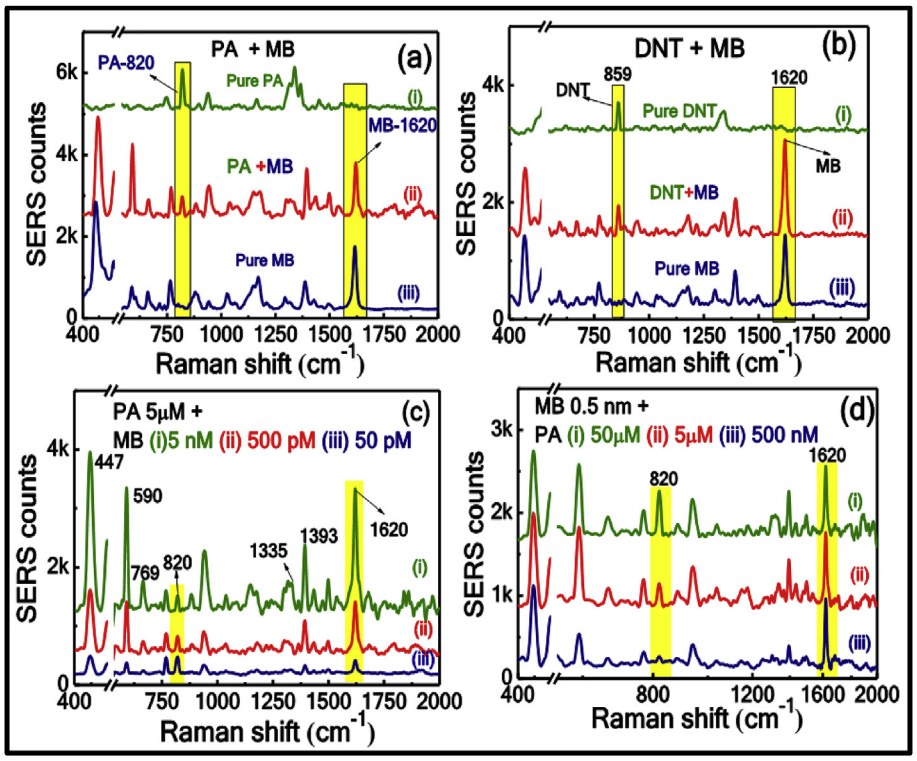

Fig. 6. SERS spectra of (a) PA + MB mixture [(i) PA 5 μM (ii) PA (5 μM)+MB (5 nM) (iii) MB (5 nM)] (b) DNT + MB mixture [(i) DNT (0.5 μM) (ii) DNT (0.5 μM) + MB (0.5 nM) (iii) MB (0.5 nM)] (c) SERS spectra of PA (5 μM) constant and different MB concentrations (i) 5 nM (ii) 500 pM (iii) 50 pM, (d) with MB (500 pM) constant and different PA concentration (i) 50 μM (ii) 5 μM (iii) 500 nM, adsorbed on the Ag–Au NPs coated Si MSA substrate, fabricated at 9.55 J/cm^2.

(500 pM), data of which is illustrated in Fig. 6(d). The intensity of MB peak at 1620 cm^{-1} was observed to be constant, but the intensity of the PA peak at 820 cm^{-1} changed (decreased) with the concentration. It was evident that Raman modes of both compounds were identified in the mixture. Additionally, we also verified the substrates homogeneity by collecting the SERS signal of PA + MB mixture at 12 random sites, and data is shown in Fig. S7(a) of the SI. The results obtained from this investigation establish that Au–Ag alloy NPs dispersed Si MSA achieve effective SERS sensitivity, high reproducibility, and constancy to detect the explosive molecules in the binary mixture form. The intensities of Raman modes corresponding to explosive molecules in mixtures are less albeit their concentration (μm) is higher in comparison to dyes (nM). This could be attributed to the (i) high Raman cross-sections of dye molecules compared to that of explosive molecules and (ii) the differences in binding affinity of molecules/analytes with the Alloy NPs with Si MSA. Few approaches have been reported for specific molecule detection in the form of mixtures [52–57]. Tian et al. [16] explored the quantitative detection of multiple analytes using graphene-based SERS (G-SERS) and showed that the concentrations, the adsorption constants, and the competing species Raman scattering cross-sections are the key factors in quantitating detection.

To evaluate the efficacy of our SERS substrate (Ag–Au alloy NPs on Si MSA), we have pushed our studies to detect the binary mixture containing two explosive molecules. The identification of explosive molecules mixed with another explosive molecule can be more challenging due to the interference and spectral overlap of different analytes. Therefore, in this study, a binary mixture of two explosive molecules, i.e., PA and DNT, were detected at various concentrations using the same SERS active substrate. The SERS spectra of pure PA, DNT and PA-DNT mixture (4 combinations) are shown in Fig. 7. The prominent peak of PA at 820 cm^{-1} and DNT at 851 cm^{-1} are highlighted with yellow and green colour rectangles. Even though both the analytes (PA, DNT) are of the same concentration (5 μM), a small variation in SERS intensities and shifts were observed. This could be attributed to the combined effect of the orientation of the analytes and interaction between the analyte molecules as well as adsorption position of analyte molecules on the generated plasmonic hotspots. The observation of prominent Raman band intensities of both molecules even at various concentrations in the binary mixture demonstrating the efficacy of Si MSA coated Ag–Au NPs substrate.

Subsequently, the Si MSA coated Ag–Au alloy NPs substrate again was employed for detecting the SERS spectra of a mixture of three molecules. A single tertiary mixture composed of two

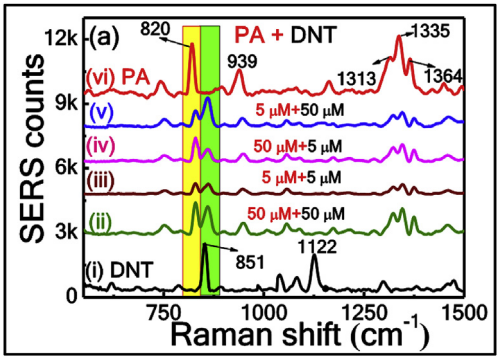

Fig. 7. SERS spectra (a) explosive mixture PA + DNT (i) DNT (50 μM) (ii) PA (50 μM) +DNT (50 μM) (iii) PA (5 μM) +DNT (5 μM) (iv) PA (50 μM) +DNT (5 μM) (v) PA (5 μM) +DNT (50 μM) and (vi) PA (50 μM), adsorbed on the Ag–Au NPs coated Si MSA substrate, fabricated at 9.55 J/cm^2.

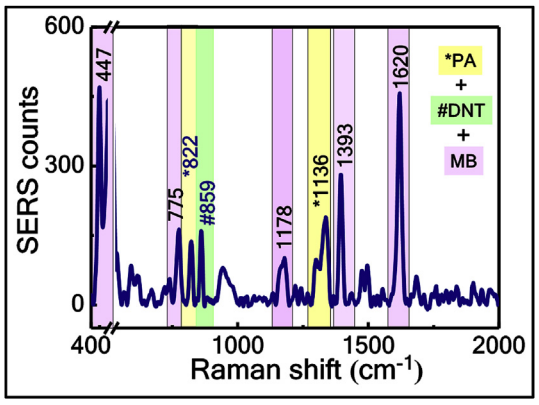

Fig. 8. SERS spectra complex mixture PA (5 μM) +DNT (5 μM) +MB (5 nM), adsorbed on the Ag–Au NPs coated Si MSA substrate, fabricated at 9.55 J/cm^2 the major characteristic peaks of PA, DNT and MB are labelled with the yellow, green and pink, respectively. (For interpretation of the references to colour in this figure legend, the reader is referred to the Web version of this article.)

explosives and a dye molecule was studied as a proof of concept for the simultaneous detection of multiple analytes using the SERS technique. Fig. 8 represents a typical SERS spectrum of the tertiary mixture containing PA (5 μM), DNT (5 μM), and MB (5 nM) as analytes. The prominent characteristic peaks of these three molecules were distinguished clearly even when the mixture was in μM concentration for explosives and nM concentration for dye molecules. The peaks are labelled with different box colours (pink for MB, yellow for PA, and green for DNT). These characteristic peaks can potentially be used for rapid screening of analytes in complex matrices. Hence, Si MSA covered with Ag–Au NPs substrate possesses potentiality for quick and convenient identification of trace-level explosive (or) organic analytes in real-time applications.

5. PCA analysis of SERS spectra

We have utilized principal component analysis (PCA), a simple statistical analysis technique for the discrimination of various explosive molecules in their pure form and mixtures with dye molecules. PCA has also been used in conjunction with other explosive detection techniques such as laser photoacoustic spectroscopy (LPAS) [58], laser-induced breakdown spectroscopy [59], and Raman spectroscopy [60,61] to discriminate explosive molecules. Li et al. utilized PCA and k nearest neighbors (KNN) for analyzing Raman spectra for the detection of colon cancer [62]. Though Raman technique (SERS) has a specific advantage of providing fingerprint spectra of various analytes, the usage of multivariate data techniques in tandem with Raman spectroscopy are conducive to robust classification and identification [63–65]. As discussed in the experimental section, the SERS response of MB, PA, RDX in pure form and MB-PA, MB-DNT, DNT-PA was recorded on Si NS (at 30 μJ) with Ag–Au NPs decorated on it. SERS spectra of the mixtures possessed the Raman modes corresponding to each analyte. The SERS spectra are baseline corrected and then analyzed for distinguishing these analytes in their pure and mixed form using a self-written, PCA code in MATLAB. The SERS spectra of six combinations, i.e., MB, PA, RDX, PA-MB, DNT-MB, PA-DNT in the 550-1750 cm^{-1} spectral range, which includes the major vibrational modes.

Fig. 9(a) depicts the PC score plot, which illustrates the obtained from PCA analysis of SERS spectra, illustrating the clustering/grouping of explosives and dye molecules in pure and mixture form. Fig. 9(b) represents the first three PCs of processed Raman spectra (SERS) explosives, dye molecules and their mixtures obtained from PCA. PCA results in principal components (PCs), which are the important spectral features that contribute demonstrate distinguishing the spectra. The first three PCs together account 89% i.e. PC1 (60%), PC2 (27%), PC3 (2%) of the variance present in the data. PC1 contains the vibrational modes from PA and MB; PC2 contains vibrational modes from MB, PA, and RDX, and PC3 contains peaks from MB, RDX, and DNT with decreasing contribution. The variance accounted can be improved by discarding the regions which do not contain major spectral peaks. Further feature selection algorithms are being developed to increase the information accounted in the multidimensional data set. Such (PCA) studies will be helpful in the cases where the signal to noise ratio is poor, and there are large number of peaks in the Raman (SERS) spectra.

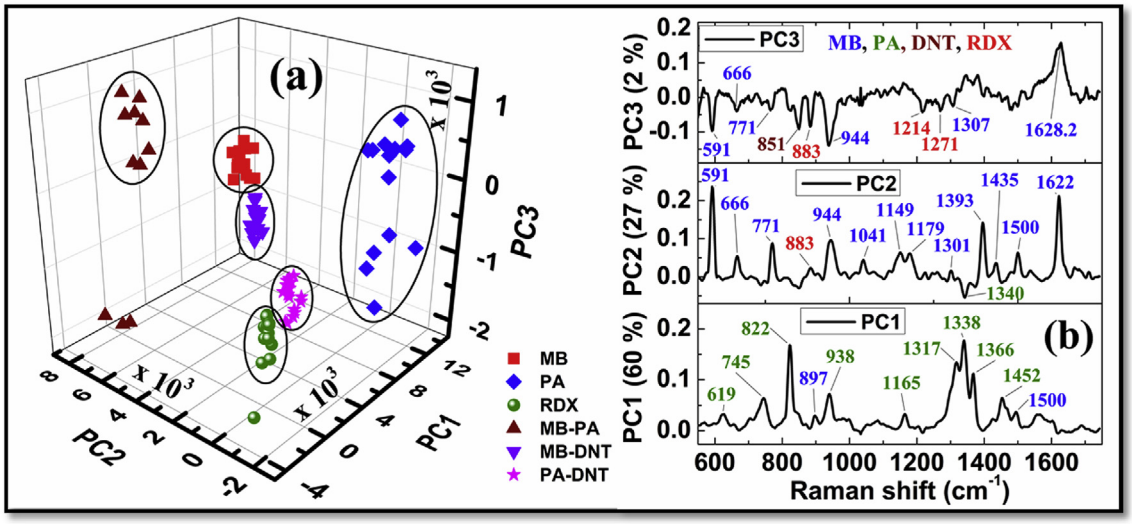

Fig. 9. (a) 3D PC plot illustrating the clustering of explosives and dye molecules in their pure and mixed forms obtained from PCA analysis on SERS spectra. (b). Principal components are contributing to the classification of explosives, dye molecules and their mixtures obtained from PCA. The vibrational modes corresponding to the molecule are indicated with the same colour for clear identification. (For interpretation of the references to colour in this figure legend, the reader is referred to the Web version of this article.)

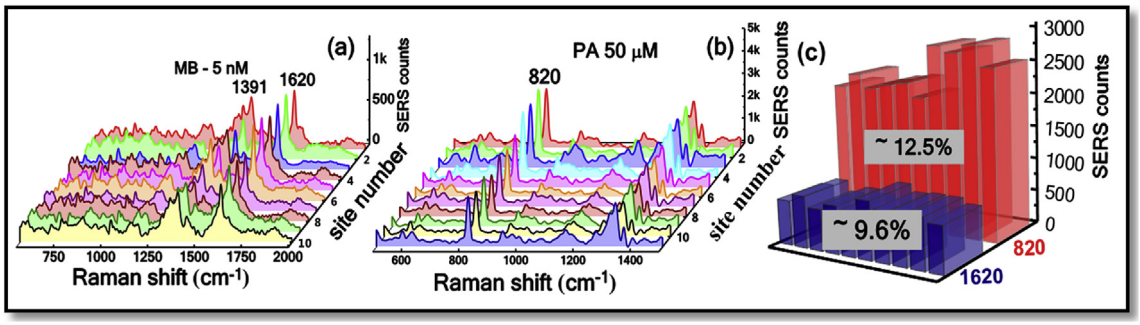

Fig. 10. SERS spectra of (a) MB (5 nM) (b) PA (50 μM) (c) the corresponding reproducibility of the SERS intensities for significant modes of MB (1620 cm^{-1}) and PA (820 cm^{-1}), respectively, using Ag-based commercial substrate from SERSitive [66].

6. Comparison with a commercial SERS substrate

In an exercise to prove the usefulness and versatility of our SERS substrate, we compared our substrate performance with a readily available commercial Ag-based SERS substrate (SERSitive) [66]. Two probe molecules (i) MB (ii) PA was considered to verify the SERS performance of these substrates. Fig. 10 (a) and (b) present the SERS spectra of MB (5 nM) and PA (50 μM). The obtained EFs were ~2.6×10^7 and ~1.2×10^4 for MB (1620 cm^{-1}) and PA (820 cm^{-1}), respectively. The observed Raman enhancement from our substrate was three orders of magnitude higher than that from a commercially available substrate. The intensity histogram representing the reproducibility of the substrate with RSD ~9.6% for MB and ~12.5% for PA, as shown in Fig. 10 (c). Our substrate has demonstrated superior performance compared to the commercially available substrate by demonstrating EFs of two order magnitude higher than the latter towards explosive detection. However, the commercially obtained SERS substrates were in transit for 3–4 weeks, and this possibly could have affected their performance. Thus, we firmly believe that the performance of hybrid SERS active substrates fabricated using femtosecond laser pulses is superior than the commercially available substrates. Further, there is scope for improvement in the enhancement factors and LOD achieved by simply tuning the morphology of the microstructures and the sizes of the alloy nanoparticles deployed in this study.

We also envisage a variety of applications for our SERS substrates. Though our main goal is towards identification of trace explosives in pure and mixed form, these can be used effectively for detection of (a) pesticides in foods (b) adulteration in oils and milk (c) forensic analysis (d) narcotics identification.

- If the analyte is a trace solid sample then one could simply use the optimized alloy nanoparticles (Si + trace analyte + drop-casted alloy nanoparticles) for detection/identification. In case the analyte cannot be transferred to the SERS substrate then simply drop-cast the alloy nanoparticles on the trace and record the SERS spectra.
- If the analyte is in liquid form then one could use nanostructured Si + drop-casted alloy nanoparticles + drop-casted analyte for superior enhancements in the SERS signals.

7. Conclusions

In summary, we demonstrate highly active SERS substrates that comprise of fs laser-generated Si MSA covered with Ag–Au alloy NPs with superior sensitivity, selectivity, and reproducibility for nitro-based explosives detection using a simple, portable spectrometer. The edges of the Si MSA facilitated the accommodation of a large number of Ag–Au NPs in the nanogaps and micro/nanocavities, which could produce a large number of hot spots and resulting in considerable enhancements in the Raman signals. The fabrication of Si MSA was performed in air at different laser fluences of 3.18–31.84 J/cm^2. The Si MSA (fabricated at 9.55 J/cm^2), which exhibited the highest enhancement for MB was utilized to probe other explosives and their mixtures. A sensitivity of 10 pM for MB (~10^{10}; typically, acceptable value for the detection of single molecule), 50 nM for PA (~10^6), and 1 μM for RDX (~10^4) was observed in their pure form. Moreover, the robustness of the substrate for multi-analyte detection was demonstrated through detection of complex mixtures of explosives and dye molecules (PA + MB, DNT + MB, and PA + DNT). The RSD values of prominent mode intensities for all the molecules being less than 15% throughout the substrate establish the reproducibility of Si MSA. Furthermore, the detection of a tertiary complex mixture (MB + PA + DNT) confirmed the potential of these substrates for real-time sensing applications. Additionally, the SERS spectra of dyes, explosives, and the complex mixtures were utilized to discriminate using principal component analysis (PCA). In future, Si NSs will be optimized by tuning the scanning speeds at constant energy and further used for the detection of explosive mixtures with more than two compounds with anisotropic metal NPs. The highly sensitive, stable, and reproducible SERS response in association with good enhancement factors articulates the tremendous potential of the Si MSA decorated with Ag–Au alloy NPs for real-time field applications. Further, large scale production of these substrates is possible thereby addressing the cost issues also.

Author contributions section

M.S.S. Bharathi: Formal analysis, Writing – original draft, Performed the ablation experiments, collected and analyzed the SERS data and writing/revision of the manuscript. B. Chandu: Formal analysis, Writing – original draft, Helped in alignment (ablation) during the experiments, assisted in the analysis of SERS data and writing/revision of the manuscript. S. Abdul Kalam: Formal analysis, Writing – original draft, Performed the PCA analysis and writing/revision of the manuscript. Syed Hamad: Conceptualization, Formal analysis, Writing – original draft, Conceptualized the project, helped in SERS data analysis and writing of the manuscript. S. Venugopal Rao: Conceptualization, Supervision, Formal analysis, Conceptualized, supervised the whole project including experiments, data analysis, writing, PCA analysis and revision of the manuscript.

Declaration of competing interest

The authors declare that they have no known competing

financial interests or personal relationships that could have appeared to influence the work reported in this paper.

Acknowledgments

VRS thanks **Mr. Paweł Albrycht**, CTO, SERSitive, Poland, for providing with the commercial SERS substrates. All the authors acknowledge DRDO, India, for funding [#ERIP/ER/1501138/M/01/319/D(R&D) dated 27.02.2017]. We also acknowledge the School of Physics, UoH, for the FESEM characterization facility.

Appendix A. Supplementary data

Supplementary data to this article can be found online at https://doi.org/10.1016/j.aca.2019.12.026.

References

[1] Y.C. Cao, R. Jin, C.A. Mirkin, Nanoparticles with Raman spectroscopic fingerprints for DNA and RNA detection, Science 297 (2002) 1536–1540.
[2] J. Feng, L. Chen, Y. Xia, J. Xing, Z. Li, Q. Qian, Y. Wang, A. Wu, L. Zeng, Y. Zhou, Bioconjugation of gold nanobipyramids for SERS detection and targeted photothermal therapy in breast cancer, ACS Biomater. Sci. Eng. 3 (2017) 608–618.
[3] A. Hakonen, P.O. Andersson, M.S. Schmidt, T. Rindzevicius, M. Käll, Explosive and chemical threat detection by surface-enhanced Raman scattering: a review, Anal. Chim. Acta 893 (2015) 1–13.
[4] M. Fan, G.F. Andrade, A.G. Brolo, A review on the fabrication of substrates for surface enhanced Raman spectroscopy and their applications in analytical chemistry, Anal. Chim. Acta 693 (2011) 7–25.
[5] M.J. Ayora, L. Ballesteros, R. Pérez, A. Rupérez, J.J. Laserna, Detection of atmospheric contaminants in aerosols by surface-enhanced Raman spectrometry, Anal. Chim. Acta 355 (1997) 15–21.
[6] M. Moskovits, Surface-enhanced spectroscopy, Rev. Mod. Phys. 57 (1985) 783.
[7] P. Lee, D. Meisel, Adsorption and surface-enhanced Raman of dyes on silver and gold sols, J. Phys. Chem. 86 (1982) 3391–3395.
[8] B. Doiron, M. Mota, M.P. Wells, R. Bower, A. Mihai, Y. Li, L.F. Cohen, N.M. Alford, P.K. Petrov, R.F. Oulton, Quantifying figures of merit for localized surface plasmon resonance applications: a materials survey, ACS Photonics 6 (2019) 240–259.
[9] T.Y. Jeon, D.J. Kim, S.-G. Park, S.-H. Kim, D.-H. Kim, Nanostructured plasmonic substrates for use as SERS sensors, Nano Converg. 3 (2016) 18.
[10] X. Liu, D. Wu, Q. Chang, J. Zhou, Y. Zhang, Z. Wang, Grooved nanoplate assembly for rapid detection of surface enhanced Raman scattering, Nanoscale 9 (2017) 15390–15396.
[11] T. Jiang, J. Song, W. Zhang, H. Wang, X. Li, R. Xia, L. Zhu, X. Xu, Au-Ag@Au hollow nanostructure with enhanced chemical stability and improved photothermal transduction efficiency for cancer treatment, ACS Appl. Mater. Interfaces 7 (2015) 21985–21994.
[12] J. Cao, T. Sun, K.T.V. Grattan, Gold nanorod-based localized surface plasmon resonance biosensors: a review, Sens. Actuators B Chem. 195 (2014) 332–351.
[13] J.Y. Xu, J. Wang, L.T. Kong, G.C. Zheng, Z. Guo, J.H. Liu, SERS detection of explosive agent by macrocyclic compound functionalized triangular gold nanoprisms, J. Raman Spectrosc. 42 (2011) 1728–1735.
[14] P. Pellacani, V. Torres-Costa, F. Agulló-Rueda, R. Vanna, C. Morasso, M. Manso Silván, Laser writing of nanostructured silicon arrays for the SERS detection of biomolecules with inhibited oxidation, Colloids Surfaces B Biointerfaces 174 (2019) 174–180.
[15] M. Alamri, R. Sakidja, R. Goul, S. Ghopry, J.Z. Wu, Plasmonic Au nanoparticles on 2D MoS2/graphene van der Waals heterostructures for high-sensitivity surface-enhanced Raman spectroscopy, ACS Appl. Nano Mater. 2 (2019) 1412–1420.
[16] H. Tian, N. Zhang, J. Zhang, L. Tong, Exploring quantification in a mixture using graphene-based surface-enhanced Raman spectroscopy, Appl. Mater. Today 15 (2019) 288–289.
[17] Y. Li, J. Dykes, N. Chopra, Silicon nanowire-gold nanoparticle heterostructures for Surface-enhanced Raman Spectroscopy, Nano-Struct. Nano-Objects 7 (2016) 12–22.
[18] Z. Huang, N. Geyer, P. Werner, J. De Boor, U. Gösele, Metal-assisted chemical etching of silicon: a review: in memory of Prof. Ulrich Gösele, Adv. Mater. 23 (2011) 285–308.
[19] C. Zhang, S.Z. Jiang, C. Yang, C.H. Li, Y.Y. Huo, X.Y. Liu, A.H. Liu, Q. Wei, S.S. Gao, X.G. Gao, Gold@ silver bimetal nanoparticles/pyramidal silicon 3D substrate with high reproducibility for high-performance SERS, Sci. Rep. 6 (2016) 25243.
[20] J. Wang, Z. Jia, C. Lv, Enhanced Raman scattering in porous silicon grating, Opt. Express 26 (2018) 6507–6518.
[21] S. Redko, A. Dolgiy, D. Zhigulin, V. Kholyavo, N. Khinevich, S. Zavatski, H. Bandarenka, Fabrication and simulation of silver nanostructures on different types of porous silicon for surface enhanced Raman spectroscopy, in: Proc. SPIE 10912, Physics and simulation of optoelectronic devices XXVII, 26 February 2019, p. 109121O.
[22] C. Novara, S. Dalla Marta, A. Virga, A. Lamberti, A. Angelini, A. Chiadò, P. Rivolo, F. Geobaldo, V. Sergo, A. Bonifacio, SERS-active Ag nanoparticles on porous silicon and PDMS substrates: a comparative study of uniformity and Raman efficiency, J. Phys. Chem. C 120 (2016) 16946–16953.
[23] H. Lin, J. Mock, D. Smith, T. Gao, M.J. Sailor, Surface-enhanced Raman scattering from silver-plated porous silicon, J. Phys. Chem. B 108 (2004) 11654–11659.
[24] G. Rao, X. Jian, W. Lv, G. Zhu, J. Xiong, W. He, A highly-efficient route to three-dimensional nanoporous copper leaves with high surface enhanced Raman scattering properties, Chem. Eng. J. 321 (2017) 394–400.
[25] S. Chang, H. Ko, S. Singamaneni, R. Gunawidjaja, V. Tsukruk, Nanoporous substrate with mixed nanoclusters for surface enhanced Raman scattering, in: APS Meeting Abstracts, vol. 54, March 2009. No. 1, Abstract ID: BAPS.2009.MAR.Z26.9.
[26] S.M. Restaino, I.M. White, A critical review of flexible and porous SERS sensors for analytical chemistry at the point-of-sample, Anal. Chim. Acta 1060 (2018) 17–29.
[27] C.-H. Lin, L. Jiang, Y.-H. Chai, H. Xiao, S.-J. Chen, H.-L. Tsai, One-step fabrication of nanostructures by femtosecond laser for surface-enhanced Raman scattering, Opt. Express 17 (2009) 21581–21589.
[28] J. Yang, J. Li, Z. Du, Q. Gong, J. Teng, M. Hong, Laser hybrid micro/nano-structuring of Si surfaces in air and its applications for SERS detection, Sci. Rep. 4 (2014) 6657.
[29] M.S.S. Bharati, B. Chandu, S.V. Rao, Explosives sensing using Ag–Cu alloy nanoparticles synthesized by femtosecond laser ablation and irradiation, RSC Adv. 9 (2019) 1517–1525.
[30] L. Tang, S. Li, F. Han, L. Liu, L. Xu, W. Ma, H. Kuang, A. Li, L. Wang, C. Xu, SERS-active Au@ Ag nanorod dimers for ultrasensitive dopamine detection, Biosens. Bioelectron. 71 (2015) 7–12.
[31] M.Y. Khaywah, S. Jradi, G. Louarn, Y. Lacroute, J. Toufaily, T. Hamieh, P.-M. Adam, Ultrastable, uniform, reproducible, and highly sensitive bimetallic nanoparticles as reliable large scale SERS substrates, J. Phys. Chem. C 119 (2015) 26091–26100.
[32] G.K. Podagatlapalli, S. Hamad, S.V. Rao, Trace-level detection of secondary explosives using hybrid silver–gold nanoparticles and nanostructures achieved with femtosecond laser ablation, J. Phys. Chem. C 119 (2015) 16972–16983.
[33] C. Byram, V.R. Soma, 2, 4-dinitrotoluene detected using portable Raman spectrometer and femtosecond laser fabricated Au–Ag nanoparticles and nanostructures, Nano-Struct. Nano-Objects 12 (2017) 121–129.
[34] K. Chang, H. Chung, Simple electrochemical synthesis of an Au–Ag–Cu trimetallic nanodendrite and its use as a SERS substrate, RSC Adv. 6 (2016) 75943–75950.
[35] L. Bi, J. Dong, W. Xie, W. Lu, W. Tong, L. Tao, W. Qian, Bimetallic gold–silver nanoplate array as a highly active SERS substrate for detection of streptavidin/biotin assemblies, Anal. Chim. Acta 805 (2013) 95–100.
[36] M. Sree Satya Bharati, C. Byram, V.R. Soma, Femtosecond laser fabricated Ag@ Au and Cu@ Au alloy nanoparticles for surface enhanced Raman spectroscopy based trace explosives detection, Front. Phys. 6 (2018) 28.
[37] H.O. Jeschke, M.E. Garcia, M. Lenzner, J. Bonse, J. Krüger, W. Kautek, Laser ablation thresholds of silicon for different pulse durations: theory and experiment, Appl. Surf. Sci. 197 (2002) 839–844.
[38] D. Tan, S. Zhou, J. Qiu, N. Khusro, Preparation of functional nanomaterials with femtosecond laser ablation in solution, J. Photochem. Photobiol. C Photochem. Rev. 17 (2013) 50–68.
[39] R. Stoian, A. Rosenfeld, I. Hertel, N. Bulgakova, E. Campbell, Comment on "Coulomb explosion in femtosecond laser ablation of Si (111)"[Appl. Phys. Lett. 82, 4190 (2003)], Appl. Phys. Lett. 85 (2004) 694–695.
[40] N. Zhang, X. Zhu, J. Yang, X. Wang, M. Wang, Time-resolved shadowgraphs of material ejection in intense femtosecond laser ablation of aluminum, Phys. Rev. Lett. 99 (2007) 167602.
[41] Z. Wu, N. Zhang, M. Wang, X. Zhu, Femtosecond laser ablation of silicon in air and vacuum, Chin. Optic Lett. 9 (2011), 093201.
[42] S. Bai, D. Serien, A. Hu, K. Sugioka, 3D microfluidic surface-enhanced Raman spectroscopy (SERS) chips fabricated by all-femtosecond-laser-processing for real-time sensing of toxic substances, Adv. Funct. Mater. 28 (2018) 1706262.
[43] H.K. Lee, Y.H. Lee, C.S.L. Koh, G.C. Phan-Quang, X. Han, C.L. Lay, H.Y.F. Sim, Y.-C. Kao, Q. An, X.Y. Ling, Designing surface-enhanced Raman scattering (SERS) platforms beyond hotspot engineering: emerging opportunities in analyte manipulations and hybrid materials, Chem. Soc. Rev. 48 (2019) 731–756.
[44] C. Byram, S.S.B. Moram, V.R. Soma, SERS based detection of multiple analytes from dye/explosive mixtures using picosecond laser fabricated gold nanoparticles and nanostructures, Analyst 144 (2019) 2327–2336.
[45] S. Almaviva, S. Botti, L. Cantarini, R. Fantoni, S. Lecci, A. Palucci, A. Puiu, A. Rufoloni, Ultrasensitive RDX detection with commercial SERS substrates, J. Raman Spectrosc. 45 (2014) 41–46.
[46] M. Ghosh, L. Wang, S.A. Asher, Deep-ultraviolet resonance Raman excitation profiles of NH_4NO_3, PETN, TNT, HMX, and RDX, Appl. Spectrosc. 66 (2012) 1013–1021.
[47] S. Lee, J. Choi, L. Chen, B. Park, J.B. Kyong, G.H. Seong, J. Choo, Y. Lee, K.-H. Shin, E.K. Lee, Fast and sensitive trace analysis of malachite green using a surface-enhanced Raman microfluidic sensor, Anal. Chim. Acta 590 (2007) 139–144.

[48] G. Krishna Podagatlapalli, S. Hamad, S.P. Tewari, S. Sreedhar, M.D. Prasad, S. Venugopal Rao, Silver nano-entities through ultrafast double ablation in aqueous media for surface enhanced Raman scattering and photonics applications, J. Appl. Phys. 113 (2013), 073106.
[49] S. Hamad, G.K. Podagatlapalli, M.A. Mohiddon, V.R. Soma, Cost effective nanostructured copper substrates prepared with ultrafast laser pulses for explosives detection using surface enhanced Raman scattering, Appl. Phys. Lett. 104 (2014) 263104.
[50] C. Byram, S.S.B. Moram, A.K. Shaik, V.R. Soma, Versatile gold based SERS substrates fabricated by ultrafast laser ablation for sensing picric acid and ammonium nitrate, Chem. Phys. Lett. 685 (2017) 103–107.
[51] S. Hamad, S.S. Bharati Moram, B. Yendeti, G.K. Podagatlapalli, S. Nageswara Rao, A.P. Pathak, M.A. Mohiddon, V.R. Soma, Femtosecond laser-induced, nanoparticle-embedded periodic surface structures on crystalline silicon for reproducible and multi-utility SERS platforms, ACS Omega 3 (2018) 18420–18432.
[52] J.J. Laserna, A.D. Campiglia, J.D. Winefordner, Mixture analysis and quantitative determination of nitrogen-containing organic molecules by surface-enhanced Raman spectrometry, Anal. Chem. 61 (1989) 1697–1701.
[53] A. Kudelski, Raman studies of Rhodamine 6G and crystal violet submonolayers on electrochemically roughened silver substrates: do dye molecules adsorb preferentially on highly SERS-active sites? Chem. Phys. Lett. 414 (2005) 271–275.
[54] J. González-Vidal, R. Perez-Pueyo, M. Soneira, S. Ruiz-Moreno, Automatic identification system of Raman spectra in binary mixtures of pigments, J. Raman Spectrosc. 43 (2012) 1707–1712.
[55] Y. Zhang, P. Yang, M.A. Habeeb Muhammed, S.K. Alsaiari, B. Moosa, A. Almalik, A. Kumar, E. Ringe, N.M. Khashab, Tunable and linker free nanogaps in core–shell plasmonic nanorods for selective and quantitative detection of circulating tumor cells by SERS, ACS Appl. Mater. Interfaces 9 (2017) 37597–37605.
[56] W.Y. Wei, I.M. White, Chromatographic separation and detection of target analytes from complex samples using inkjet printed SERS substrates, Analyst 138 (2013) 3679–3686.
[57] A.B. Zrimsek, N.L. Wong, R.P. Van Duyne, Single molecule surface-enhanced Raman spectroscopy: a critical analysis of the bianalyte versus isotopologue proof, J. Phys. Chem. C 120 (2016) 5133–5142.
[58] G. Giubileo, F. Colao, A. Puiu, Identification of standard explosive traces by infrared laser spectroscopy: PCA on LPAS data, Laser Phys. 22 (2012) 1033–1037.
[59] A.K. Shaik, N.R. Epuru, H. Syed, C. Byram, V.R. Soma, Femtosecond laser induced breakdown spectroscopy based standoff detection of explosives and discrimination using principal component analysis, Opt. Express 26 (2018) 8069–8083.
[60] K. Konstantynovski, G. Njio, F. Börner, A. Lepcha, T. Fischer, G. Holl, S. Mathur, Bulk detection of explosives and development of customized metal oxide semiconductor gas sensors for the identification of energetic materials, Sens. Actuators B Chem. 258 (2018) 1252–1266.
[61] X. He, Y. Liu, S. Huang, Y. Liu, X. Pu, T. Xu, Raman spectroscopy coupled with principal component analysis to quantitatively analyze four crystallographic phases of explosive CL-20, RSC Adv. 8 (2018) 23348–23352.
[62] X. Li, T. Yang, S. Li, D. Wang, Y. Song, S. Zhang, Raman spectroscopy combined with principal component analysis and k nearest neighbour analysis for non-invasive detection of colon cancer, Laser Phys. 26 (2016), 035702.
[63] J.-Y. Lim, J.-S. Nam, H. Shin, J. Park, H. Song, M. Kang, K. Lim, Y. Choi, Identification of newly emerging influenza viruses by detecting the virally infected cells based on surface enhanced Raman spectroscopy (SERS) and principal component analysis (PCA), Anal. Chem. 91 (9) (2019) 5677–5684.
[64] J. Hwang, N. Choi, A. Park, J.-Q. Park, J.H. Chung, S. Baek, S.G. Cho, S.-J. Baek, J. Choo, Fast and sensitive recognition of various explosive compounds using Raman spectroscopy and principal component analysis, J. Mol. Struct. 1039 (2013) 130–136.
[65] S. Botti, S. Almaviva, L. Cantarini, A. Palucci, A. Puiu, A. Rufoloni, Trace level detection and identification of nitro-based explosives by surface-enhanced Raman spectroscopy, J. Raman Spectrosc. 44 (2013) 463–468.
[66] https://www.sersitive.eu/.